Journal Name

ARTICLE TYPE

Cite this: DOI: 10.1039/xxxxxxxxxx

Self-cleaning, high transmission, near unity haze OTS/silica nanostructured glass

Sajad Haghanifar,[a] Ping Lu,[b] Md Imrul Kayes,[a]Susheng Tan,[c]Ki-Joong Kim,[b]Tongchuan Gao,[a]Paul Ohodnicki,[b] and Paul W Leu*[a,d]

Received Date
Accepted Date

DOI: 10.1039/xxxxxxxxxx

www.rsc.org/journalname

High haze, high transparency substrates can increase the power conversion and extraction efficiency of solar cells and light emitting diodes (LEDs), respectively. In this paper, we demonstrate a new octadecyltrichlorosilane (OTS)/silica nanostructured substrate that displays high transmission (91.5 ± 0.5% at 550 nm wavelength) and near unity haze (98.1 ± 0.5% at the same wavelength) with 143° scattering angle. The OTS/silica nanostructures are fabricated through a scalable and facile maskless reactive ion etching (MRIE) process followed by OTS coating. The OTS coating enhances the transmission of the structures by merging silica nanostructures together by capillary forces and effectively grading the index of refraction. The OTS/silica nanostructures display the highest combination of both transmission and haze in the literature as defined by Pareto optimality. The OTS/silica nanostructured glass exhibits lotus leaf-like wetting with a $159.7 \pm 0.6°$ water contact angle (WCA) and $4.9 \pm 0.6°$ contact angle hysteresis. We demonstrate the structures have self-cleaning functionality where about 100% of transparency can be easily recovered after graphite soiled substrates are rinsed with water. This self-cleaning functionality is maintained after 200 cycles of soiling and cleaning. The OTS/silica nanostructured glass may be an important substrate in optoelectronic applications where a combination of high transmission, high haze, and self cleaning function are important.

Introduction

Optoelectronic substrates with high transmission and high light scattering are needed for optoelectronic applications such as solar cells and light emitting diodes (LEDs) where the substrate can increase how much light scatters into or out of the underlying photoactive layers, respectively[1,2]. These substrates can enhance the power conversion efficiency of solar cells and extraction efficiency of LEDs. Various paper substrates have been demonstrated for optoelectronic applications including mesoporous wood cellulose paper[3], microsized wood fibers in paper[4], nanostructured paper[5], wood composites[6], and plastic-paper[1]. While paper may offer new functionality for optoelectronic applications such as flexibility, glass is most frequently used for optoelectronic devices due to its low cost and moisture barrier properties. High transparency, high haze glass substrates have included self-aggregated alumina nanowire arrays on glass[7], imprinted polydimethylsiloxane (PDMS) coatings on glass[8], and our recent nanograss glass[9]. Optoelectronic substrates would also benefit from self-cleaning properties where particulates are easily removed from the surface upon application of water. Dust or dirt particulates may accumulate on the surface and reduce the transmission of light and can significantly reduce the power conversion and extraction efficiency of solar cells and LEDs, respectively[10,11]. There is a need to develop substrates for advanced optoelectronic applications that exhibit high haze and high transparency and self-cleaning function.

In this paper, we report on self cleaning octadecyltrichlorosilane (OTS)/silica nanostructured glass which exhibits both high transparency and near unity haze. The OTS/silica nanostructures are synthesized by a facile maskless reactive ion etching method (MRIE) to create silica nanograss blades followed by OTS coating. The OTS/silica nanostructured glass exhibits a transparency of 91.5 ± 0.5% with a haze value of 98.1 ± 0.5% at a wavelength of 550 nm. The OTS coating enhances the transparency of the nanograss glass by as much as over 10% as the silica nanograss blades merge together from capillary forces during coating and effectively grade the index of refraction between the air and the glass. Furthermore, the OTS coating does not signifi-

[a] Department of Industrial Engineering, University of Pittsburgh, Pittsburgh, PA 15261, USA; E-mail: pleu@pitt.edu
[b] National Energy Technology Laboratory, U.S. Department of Energy, Pittsburgh, PA 15236, USA.
[c] Department of Electrical and Computer Engineering, University of Pittsburgh, Pittsburgh, PA 15261, USA.
[d] Department of Mechanical Engineering, University of Pittsburgh, Pittsburgh, PA 15261, USA.

cantly change the haze. The glass exhibits strong light scattering ability with a scattering angle of 143°. Our OTS/silica nanostructured glass demonstrates the highest combination of haze and transmission in the literature as defined by Pareto optimality.

The silica nanograss glass is superhydrophilic initially with a water contact angle (WCA) of $7.4 \pm 0.2°$. After coating, the OTS/silica nanostructures become superhydrophobic with a WCA of $159.7 \pm 0.6°$ due to a combination of the nanostructures and low surface energy OTS. The OTS coated glass exhibits lotus leaf-like wetting with high WCA and $4.9 \pm 0.6°$ contact angle hysteresis. We demonstrate the structures have self-cleaning functionality where about 100% of the original transparency can be easily recovered after graphite soiled substrates are rinsed with water. The original transparency and haze of the substrates are recovered after as many as 200 cycles of soiling and cleaning. The combination of optical properties and self-cleaning functionality make the nanostructured hazy glass an strong candidate for several optoelectronic applications.

Experimental

Nanostructured hazy glass fabrication process

Reactive ion etching (RIE) was used to etch fused silica. In the RIE chamber, a plasma and polymer composition is generated [12] and radicals and ions bombard the substrate. Polymer particles are deposited on the surface of the substrate during the etching process, which acts as a nano-mask which creates high aspect-ratio nanograss [13]. The fused silica is etched by a CHF_3, SF_6, and Ar chemistry, where the etching parameters and conditions have been reported previously [9]. In general, the pressure, power and flow rate of the etching gases can be selected and varied, such as to tune or control the etch rate and the resulting morphology of the nano-patterned textures created on the surface of the fused silica substrate which allows the haze and transparency of the substrate to be tuned, controlled and maximized. The overall height and density of the pattern can vary. Typically, the height of each individual grass-like structure is consistent. Furthermore, the distance between the blades is also consistent.

OTS coating process

Before coating the glass surface, the samples were cleaned. Then 0.2% OTS solution in toluene was prepared. The glass surfaces were inserted in OTS solution for 17 minutes and then the glass surfaces were transferred to a beaker containing only toluene in order to remove excess OTS from it. After 5 minutes, the samples were taken out and dried using a nitrogen pressure gun. After that, the samples were placed on a hot plate set at 90 °C for half an hour. Finally, samples were transferred to toluene solution and sonicated for 5 minutes, followed by drying with a nitrogen gun.

TEM imaging

Transmission electron microscopy (TEM) images and electron diffraction spectroscopy (EDS) spectra were acquired using a JEOL JEM-2100F TEM operated at 200 kV and equipped with an OXFORD Aztec windowless x-ray energy dispersive spectrometer. The TEM specimens were prepared using a focused ion beam (FIB)/scanning electron microscope dual beam system (ThermoFisher). A Pt layer was deposited on top of the region of interest, and a wedge region was ion milled. Then this small section was removed using a microprobe and attached to a TEM grid for imaging.

Optical and surface roughness Characterization

A spectrophotometer (PerkinElmer, Lambda 1050) equipped with a 150 mm integrating sphere was used for measuring the optical characteristics of the samples. The scattering angular distribution was measured using Cary 7000 Universal Measurement Spectrophotometer (UMS); In this instrument, incident light is normal to the sample surface with a 5 mm × 5 mm square beam and the photodetector is scanning from 10 to 350 (-10)°; the wavelength scan is from 530 to 570 nm and the wavelength of 550 nm is selected to obtain the data. In order to study the surface roughness, optical profilometry (Contour GT Bruker) was used. The scan distance of profilometry was set on 400 μm × 800 μm and the measurements have been done for ten times, then average and standard deviation for each sample has been calculated.

Self Cleaning Characterization

For self-cleaning test, the transmission of substrates of about 5 cm^2 area were measured in the original state, soiled state, and after cleaning. The initial transmission of different types of glasses were obtained using a spectrophotometer (PerkinElmer, Lambda 1050). After that, 0.5 gram graphite powder from Aldrich chemistry company with particle size less than 150 μm, 99.99% trace metal base was placed on top surface of the glass, then ultrasonicated for 5 min to disperse the powder on the surface, in room temperature. The transmission of the soiled state was measured. For cleaningt, 2 ml of water was dropped onto the glass and the transmission was measured afterwords.

Results and Discussion

Figure 1 shows details of the fabrication process and structure of the OTS/silica nanostructured glass. Figure 1(a) shows a schematic of the fabrication process. The fused silica substrate is etched by a maskless RIE process to create nanograss glass [9] and then coated with OTS. Details of the fabrication process are provided in the Methods section. Figure 1(b) shows a 10° tilted cross section scanning electron microscope (SEM) images of 8.5 ± 0.2 μm initial height hazy glass (i) before and (ii) after OTS modification, respectively. While the initial structures are about 8.5 ± 0.2 μm long, the OTS deposits in the space between nanograss blades. In some cases where the nanograss blades are close together, the drying process merges the blades together by capillary-induced bending [7,14]. The final height of the structures after OTS coating is only about 2.2 ± 0.2 μm long. Figure 1(c) shows overhead SEM images of 8.5 ± 0.2 μm initial height hazy glass (i) before and (ii) after OTS modification, respectively. The reduced density of structures is apparent in these images as various nanograss blades have merged together therefore the surface roughness slightly decreases. Figure 1(d)(i) shows a transmission electron microscopy (TEM) image of a selected area of the

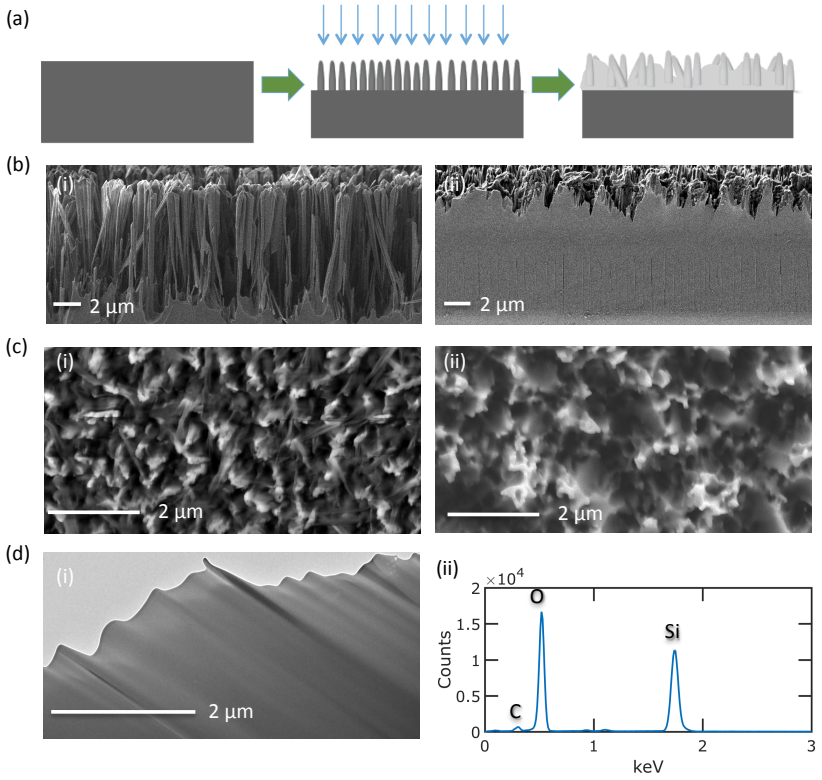

Fig. 1 (a) Fabrication process of etching silica nanostructures with RIE followed by OTS coating. (b) 10°tilted cross section SEM images of 8.5 ± 0.2 μm height hazy glass (i) before and (ii) after OTS modification. (c) Overhead SEM images of 8.5 ± 0.2 μm height hazy glass (i) before and (ii) after OTS modification, (d) (i) TEM image and (ii) EDS spectrum of OTS coated hazy glass with 8.5 ± 0.2 μm initial blade height.

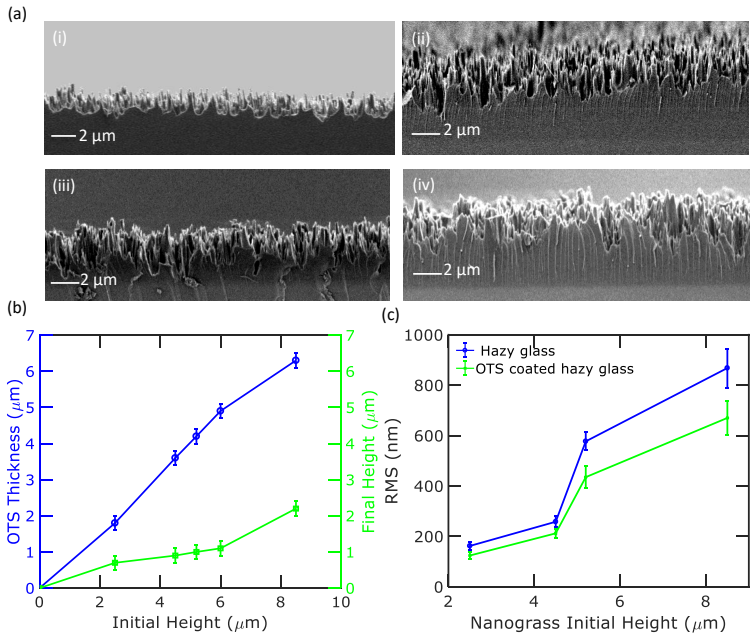

8.5 ± 0.2 μm initial height OTS coated hazy glass near the tips and Figure 1(d)(ii) plots the energy-dispersive x-ray spectroscopy (EDS) analysis of this selected area. After hydrolysis of the chlorine groups in the OTS, the molecules attach to the surface and polymerization takes place with elimination of water[15]. The final surfaces are terminated by methyl groups. The structures are primarily silica with some carbon from the carbon chains in the OTS. The small peaks near 0.9 keV and 1.1 keV correspond to the Cu La line and Na Ka line, respectively. The Cu and Na measurements come from the support grid and glass respectively.

Different height nanograss glass were fabricated by varying the RIE time followed by OTS deposition. Figure 2(a) shows cross section SEM images of the OTS/silica nanostructured glass of different initial heights of (i) 2.5 ± 0.2, (ii) 4.5 ± 0.2, (iii) 5.2 ± 0.2, and (iv) 8.5 ± 0.2 μm. After OTS deposition, the final height of the structures are about (i) 0.7 ± 0.2, (ii) 0.9 ± 0.2, (iii) 1.0 ± 0.2, and (iv) 2.2 ± 0.2 μm as the OTS fills the space between the nanostructures. All the measurement are the average and standard deviation of three different measurements in different cross sections of samples. Figure 2(b) shows a plot on the left y-axis of how the OTS thickness varies as a function of initial nanograss height and on the right y-axis how the final structure height varies as a function of initial nanograss height. The optical properties of the various samples were subsequently characterized. The root mean square (RMS) of the surface roughness for different height hazy glass before and after OTS coating is shown in Figure 2(c). It is apparent that after OTS coating of hazy glass, the surface roughness slightly decrease for all initial heights due to merged blades together.

Figure 3(a) shows the total transmission as a function of wavelength for the nanostructured hazy glass both (i) before and (ii) after OTS coating. Figure 3(b) shows the total transmission of the various structures at 550 nm wavelength. The transmission of bare fused silica is 93.2% both before and after OTS modification. On these surfaces, the OTS only forms a monolayer[15–18] and has negligible change on the transmission of the original fused silica across the entire spectrum. For the 2.5 ± 0.2 μm nanograss glass, the transmission is initially $91.8 \pm 0.5\%$ at 550 nm wavelength. After OTS modification, the transmission increases to $92.4 \pm 0.5\%$. The improvements in transmission are primarily in the wavelengths under 600 nm. Nanograss glass with initial heights 4.5 ± 0.2 μm and above (final height over 0.9 ± 0.2 μm) demonstrate an improvement in transparency across the entire spectrum after OTS coating compared to before. The enhancement in transmission from the OTS coating is shown in Fig. 3(c) and over $8.0 \pm 0.5\%$ at a initial silica nanostructure height of 5.2 ± 0.2 μm and longer (final OTS/silica height over 1.0 ± 0.2 μm). This improvement in enhancement is primarily due to the merging of nanograss blades. While the initial blades are structures of constant diameter, after OTS deposition, structures that are close together are merged together. These sub-wavelength structures effectively grade the index of refraction of the glass such that the antireflection and thus, transmission properties are improved.

Next, we characterized the haze factor of the original nanograss glass and compared it with the OTS/silica nanostructured glass. The haze factor is defined as the percent of scattered transmission to the total transmission:

$$H(\lambda) = \left[\frac{\text{Scattered transmission}(\lambda)}{\text{total transmission}(\lambda)} \right] \times 100\% \qquad (1)$$

where λ is the free space wavelength. The portion of the total transmitted light that is considered scattered transmission is transmitted light that deviates from the incident beam greater than 2.5°as defined by the ASTM D1003 standard[19]. Figure 4(a) plots the haze of (i) the original nanograss glass, and (ii) the OTS/silica core-shell nanograss glass. The haze in the silica/OTS core-shell nanograss glass increases monotonically with height similar to that of just the silica nanograss glass, and the haze does not change much prior to and after OTS coating. The haze is near unity at wavelengths in the ultraviolet and visible, though the haze does start to drop slightly in the near-infrared.

We next characterized the angular distribution of the transmission through various substrates. Figure 4(b) shows the scattering angular distribution of transmission at a wavelength of 550 nm for (i) bare glass before and after OTS modification and (ii) 5.2 ± 0.2 μm initial height hazy glass before and after OTS coating. As can be seen from these plots, the OTS coating does not change the haze substantially in either sample. On bare glass, the OTS only forms a monolayer[20] and does not change the haze as expected. On the nanograss glass, the OTS also does not change the haze significantly. While the OTS reduces the height of the structures and merges some of the silica structures together, the structures are also heterostructures now with silica nanostructures and OTS coating. These additional interfaces may compensate for the reduced scattering from reduced roughness. The scattering angle range, defined as the range of angles in which lights have more than 5% intensity of the highest intensity at 0° was also characterized from these plots[5]. The scattering angle ranges of the bare silica and OTS-coated silica at wavelength of 550 nm are both 7°. The photodetector receives light in a 6°cone so that there is substantial broadening on the light intensities measured and the haze calculated directly from these plots differ from those measured with an integrating sphere. The haze of these samples at 550 nm are both less than 1%. For the 5.2 ± 0.2 μm height hazy nanograss glass, the scattering angle range is 146°initially and 143°after OTS coating. The haze of these samples are $98.5 \pm 0.5\%$ and $98.1 \pm 0.5\%$, respectively.

Figure 5 plots the the total transmission and haze (at 550 nm) for a variety of optoelectronic substrates. For each type of substrate, only the best performing data (as defined by Pareto optimality) is plotted. The Pareto frontier is the set of solutions where one attribute cannot be improved without degrading another attribute. Our experimental data for the nanograss glass is plotted with green circles and our data for the OTS/silica nanostructures is plotted with blue squares. For comparison purposes, we plot the best performing optoelectronic substrate data in the literature for glass substrates using yellow markers and other optoelectronic substrates using gray markers. Glass substrates have been modified using aggregated alumina nanowire arrays[7] and imprinted PDMS on glass[8]. In addition, a variety of paper substrates have been demonstrated such as mesoporous wood cellu-

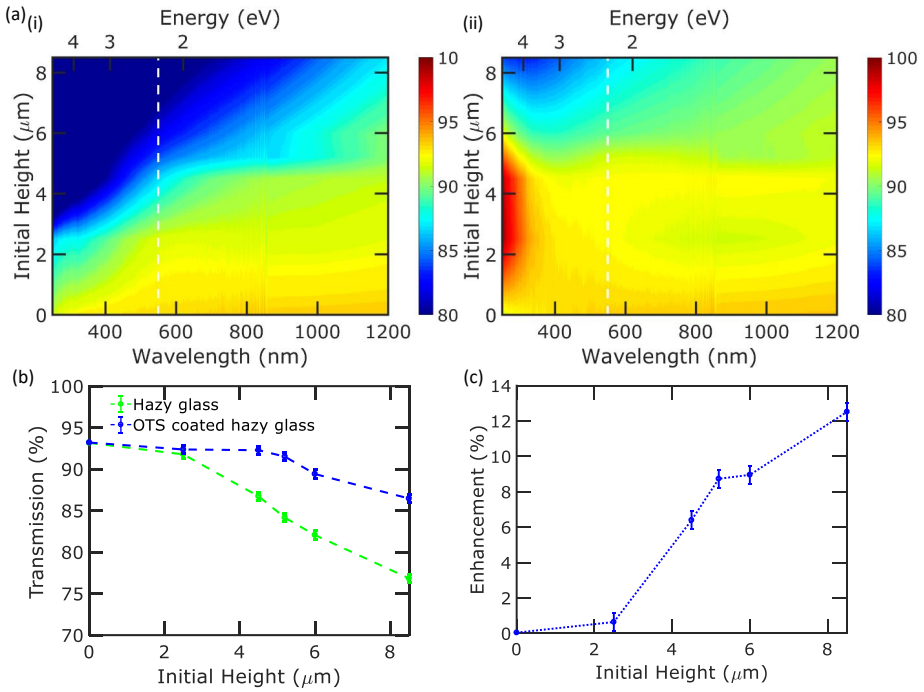

Fig. 3 Contour plots of (a) total transmission (%) (i) of nanograss glass (ii) and core/shell silica/OTS nanograss glass. (b) Plot of total transmission at 550 nm wavelength as a function of initial blade height. (c) Enhancement in transmission after OTS coating.

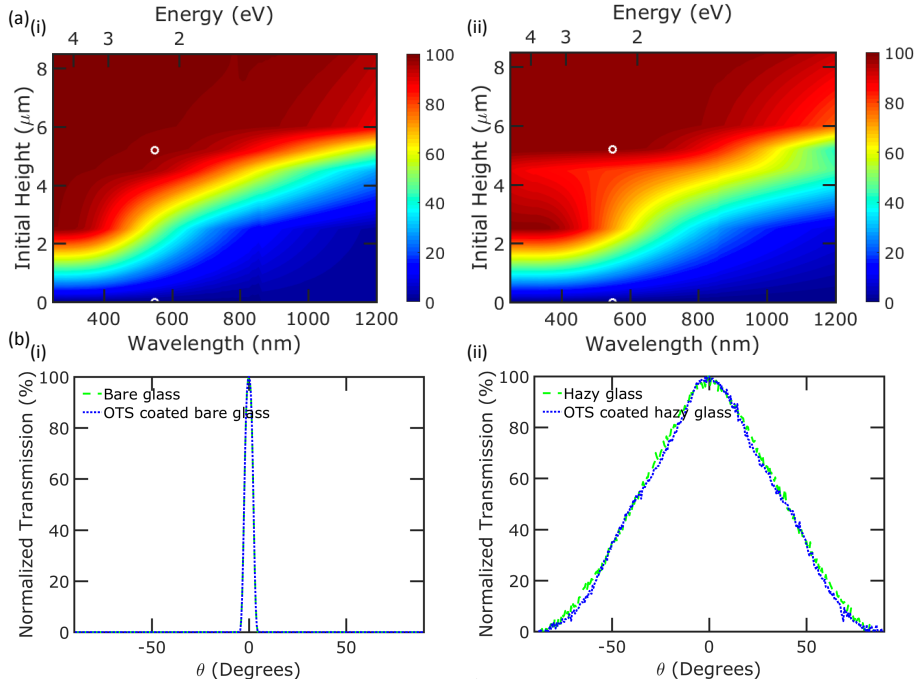

Fig. 4 Haze contour plots of (a)(i) nanograss glass and (ii) core/shell nanogrss. (b) ADF plots of (i) Smooth glass and (ii) 5.2 ± 0.2 μm height hazy glass without and with OTS layer.

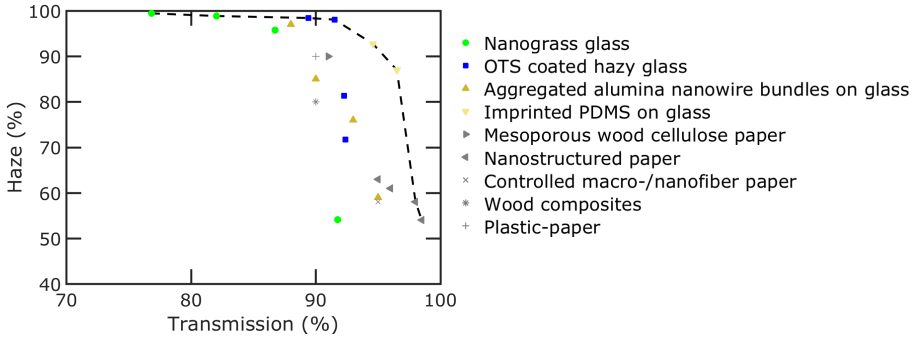

Fig. 5 Haze versus transmission for substrates at $\lambda = 550$ nm. Our hazy glass data with and without OTS layer is shown. The best data for aggregated alumina nanowire arrays on glass[7], imprinted PDMS on glass[8], mesoporous wood cellulose paper[3], controlled macro/nanofiber paper[4], nanostructured paper[5], wood composites[6], and plastic-paper hybrids[1] are also shown. The Pareto frontier of all the data is marked with a dashed line.

	Bare glass	OTS coated glass	Nanograss glass	OTS/silica nanostructured glass
Water droplet shape	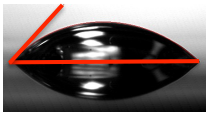	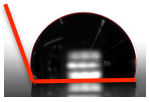		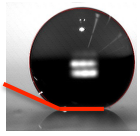
Static water contact angle (degrees)	42.9 ± 1.1	108.5 ± 0.7	7.4 ± 0.2	159.7 ± 0.6
Contact angle hysteresis (degrees)	35.5 ± 2.7	19.5 ± 1.7	-	4.9 ± 0.6

Fig. 6 Water contact angle of bare glass, OTS coated bare glass, 5.2 ± 0.2 μm height nanograss glass, and 5.2 ± 0.2 μm initial height OTS/silica nanostructured glass.

lose paper[3], controlled macro/nanofiber paper[4], nanostructured paper[5], wood composites[6], and plastic-paper hybrids[1]. For the nanograss glass samples, two of the nanograss glass samples reside on the Pareto frontier. The 8.5 ± 0.2 μm height nanograss glass exhibits $76.8 \pm 0.5\%$ transmission and $99.4 \pm 0.5\%$ haze, and the 6.0 ± 0.2 μm height nanograss glass has $82.1 \pm 0.5\%$ transmission and $98.9 \pm 0.5\%$ haze. Other Pareto optimal structures include imprinted PDMS on glass with 94.6% transparency and 92.7% haze and 96.5% transparency and 87% haze[8]. Our OTS/silica nanostructured glass demonstrates the highest combination of transmission and haze as well. The 6.0 ± 0.2 μm and 5.2 ± 0.2 μm initial height (1.1 ± 0.2 and 1.0 ± 0.2 μm final height, respectively) OTS/silica nanostructures have $89.4 \pm 0.5\%$ transmission and $98.4 \pm 0.5\%$ haze and $91.5 \pm 0.5\%$ transmission and $98.1 \pm 0.5\%$ haze, respectively.

For a surface to be self-cleaning, it needs to have a combination of superhydrophobicity (WCA $> 150°$) and small contact angle hysteresis[21]. We next compare how the OTS modifies the wetting of various surfaces. Figure 6 shows the static WCA and hysteresis of bare glass, OTS coated bare glass, 5.2 ± 0.2 μm height nanograss glass, and 5.2 ± 0.2 μm initial height (1.0 ± 0.2 μm final height) OTS/silica nanostructured glass. The hysteresis is the difference between the advancing and receding contact angle. The bare fused silica is hydrophilic with a WCA of $42.9 \pm 1.1°$. After OTS coating, the glass becomes hydrophobic as the WCA increases to $108.5 \pm 0.7°$. However, the OTS coating on bare glass is not enough to make the bare glass sample superhydrophobic. In contrast, nanostructures have been demonstrated to increase superhydrophilicity and superhydrophobicity[22–25]. The nanograss glass is superhydrophilic with a contact angle of $7.4 \pm 0.2°$as the nanostructuring enhances the Wenzel state of wetting. After OTS coating, the wetting of the nanostructures becomes superhydrophobic with a WCA of $159.7 \pm 0.6°$. The nanostructures promote Cassie-Baxter wetting where air pockets increase the apparent static water contact angle. The hysteresis is only $4.9 \pm 0.6°$, which is indicative of weak water adhesion with the surface. When the OTS/silica nanostructured glass is tilted just slightly, the droplets easily roll off. The rolling angle was measured as $1.5 \pm 0.5°$.

To study the self-cleaning functionality of the different types of glass, we performed self-cleaning tests where samples were soiled with graphite powder and then rinsed with water. Self-cleaning is defined here as the application of water without any additional scrubbing. Glass substrates of about 5 cm^2 area were soiled with 0.5 grams of graphite powder and then rinsed with 2 mL of water. The total transmission of the samples was measured initially, after soiling, and finally, after cleaning. Figure 7 summarizes these self-cleaning results. Figure 7(a) shows the transmission spectra and figure 7(b) shows optical images of the (i) bare glass, (ii) OTS coated bare glass, and (iii) OTS/silica nanostructured glass in the original state, after soiling, and after cleaning. Three measurements were made for each sample and the mean and standard

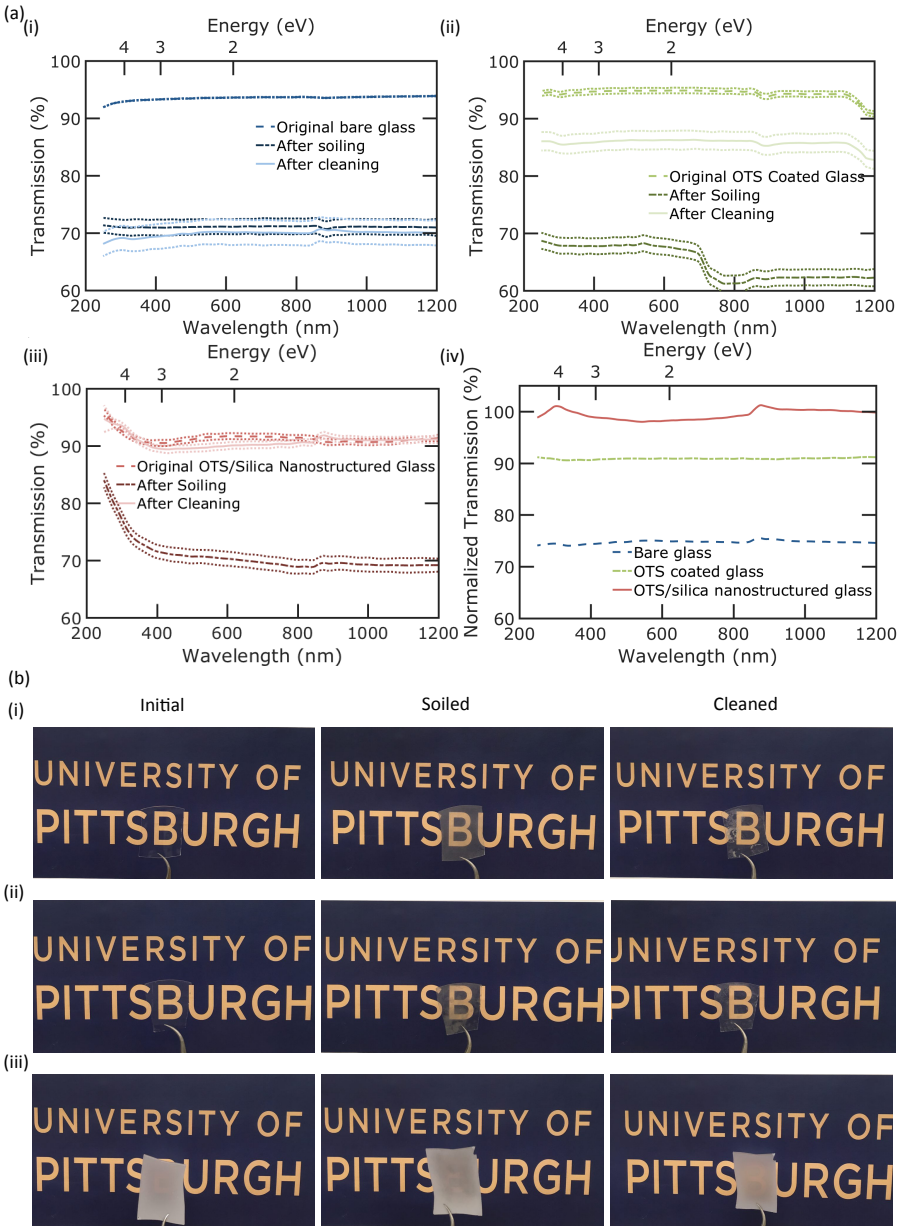

Fig. 7 (a) Total transmission plots as a function of wavelength for (i) flat fused silica, (ii) OTS coated flat fused silica and (iii) $5.2 \pm 0.2\ \mu m$ height OTS coated nanograss glass in three different states. (a) (iv) plots the normalized transmission of the various glass substrates showing the mean transmission after cleaning relative to the original mean transmission. (b) Shows Optical images of (i) flat fused silica, (ii) OTS coated flat fused silica and (iii) $5.2 \pm 0.2\ \mu m$ height OTS coated nanograss glass in initial, soiled and cleaned states.

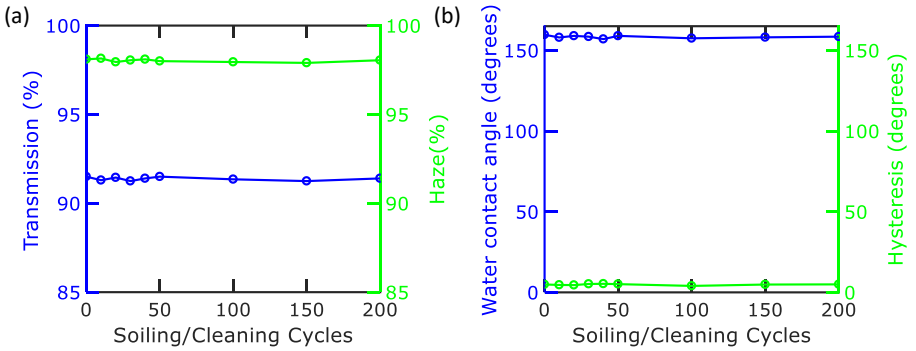

Fig. 8 (a) Transmission (left y-axis) and haze (right y-axis) at 550 nm wavelength as a function of soiling/cleaning cycle for 5.2 ± 0.2 μm initial height OTS/silica nanostructured glass. (b) Water contact angle (left y-axis) and hysteresis (right y-axis) as a function of soiling/cleaning cycle for 5.2 ± 0.2 μm initial height OTS/silica nanostructured glass.

deviation for each state are also shown. For the bare glass, no improvement in transmission was observed after cleaning with water. The standard deviation becomes larger due to decreased uniformity in the transmission as the graphite tended to agglomerate into patches as can be seen in Fig. 7(b). In contrast, the OTS coated bare glass shows some improvement in transmission after cleaning, but does not recover its original transmission. Finally, the OTS/silica nanostructured glass decreases similarly to the other two samples, but the transmission almost recovers back to its original state after rinsing.

Figure 7(a)(iv) plots the normalized transmission of the various glass substrates showing the mean transmission after cleaning relative to the original mean transmission. The bare glass transmission is about 75% of its original value across all wavelengths after cleaning which is about the same as what it is in the soiled state. In contrast, the soiled OTS coated bare glass recovers about 91% of its original transmission after cleaning. Finally, the OTS/silica nanostructured glass not only demonstrates the best anti-fouling properties as its transmission decreases the least in the soiled state, but self-cleaning, where the transmission is about 100% of its original value. Due to statistical variation, the transmission after cleaning is, in fact, over 100% of its original value and in some parts of the spectrum measured and slightly below 100% in others.

In order to study the long term functionality of self-cleaning glass, the same soiling and cleaning procedure were performed up to 200 cycles and the transmission and haze at 550 nm and the WCA and hysteresis were measured. Figure 8(a) plots transmission at 550 nm (left y-axis) and haze (right y-axis) at 550 nm wavelength as a function of cleaning cycle for 5.2 μm initial height OTS/silica nanostructured glass. There were no significant changes in both transmission and haze after 200 cycles of soiling and cleaning. Figure 8(b) plots the WCA (left y-axis) and hysteresis (right y-axis) as a function of cleaning cycle for 5.2 μm initial height OTS/silica nanostructured glass. The WCA and hysteresis were also maintained after up to 200 cycles of soiling and cleaning. These experiments demonstrate that the durability of the self-cleaning glass is promising.

Conclusion

In conclusion, we demonstrated self-cleaning, high transmission, near unity OTS/silica nanostructured glass. The 5.2 ± 0.2 μm initial height OTS/silica nanostructured glass showed $91.5 \pm 0.5\%$ total transparency and $98.1 \pm 0.5\%$ haze and 143° scattering angle at 550 nm wavelength. The wetting went from superhydrophilic to superhydrophobic after OTS coating. The OTS/silica nanostructures demonstrate high water contact angle and low contact angle hysteresis. The samples demonstrate self-cleaning functionality where graphite soiled substrates recover about all of their transparency after rinsing with water. This characteristics make the superhydrophobic hazy glass a strong candidate to use in optoelectronic applications such as solar cells and LEDs which combination of high transmission, high haze, and self cleaning function are important requirements.

Conflicts of interest

There are no conflicts to declare.

Acknowledgements

This work was supported in part by the National Science Foundation (ECCS 1552712)..

References

1 Y. Yao, J. Tao, J. Zou, B. Zhang, T. Li, J. Dai, M. Zhu, S. Wang, K. KelvinÂ Fu, D. Henderson, E. Hitz, J. Peng and L. Hu, *Energy & Environmental Science*, 2016, **9**, 2278–2285.

2 G. Tongchuan, H. Sajad, L. M. G., L. Ping, K. M. Imrul, P. B. D., Z. Ziyu, O. P. R. and L. P. W., *Advanced Optical Materials*, **6**, 1700829.

3 H. Zhu, Z. Fang, Z. Wang, J. Dai, Y. Yao, F. Shen, C. Preston, W. Wu, P. Peng, N. Jang, Q. Yu, Z. Yu and L. Hu, *ACS Nano*, 2016, **10**, 1369–1377.

4 Z. Fang, H. Zhu, W. Bao, C. Preston, Z. Liu, J. Dai, Y. Li and L. Hu, *Energy & Environmental Science*, 2014, **7**, 3313–3319.

5 Z. Fang, H. Zhu, Y. Yuan, D. Ha, S. Zhu, C. Preston, Q. Chen, Y. Li, X. Han, S. Lee, G. Chen, T. Li, J. Munday, J. Huang and L. Hu, *Nano Lett.*, 2014, **14**, 765–773.

6 M. Zhu, T. Li, C. S. Davis, Y. Yao, J. Dai, Y. Wang, F. AlQatari, J. W. Gilman and L. Hu, *Nano Energy*, 2016, **26**, 332–339.

7 G. Kang, K. Bae, M. Nam, D.-H. Ko, K. Kim and W. J. Padilla, *Energy & Environmental Science*, 2015, **8**, 2650–2656.

8 W.-P. Chu, J.-S. Lin, T.-C. Lin, Y.-S. Tsai, C.-W. Kuo, M.-H. Chung, T.-E. Hsieh, L.-C. Liu, F.-S. Juang and N.-P. Chen, *Optics Communications*, 2012, **285**, 3325–3328.

9 S. Haghanifar, T. Gao, R. T. R. D. Vecchis, B. Pafchek, T. D. B. Jacobs and P. W. Leu, *Optica*, 2017, **4**, 1522–1525.

10 D. Goossens and E. Van Kerschaever, *Solar Energy*, 1999, **66**, 277–289.

11 P. D. Burton, A. Hendrickson, S. S. Ulibarri, D. Riley, W. E. Boyson and B. H. King, *IEEE Journal of Photovoltaics*, 2016, **6**, 976–980.

12 S. Haghanifar, R. T. R. D. Vecchis, K.-J. Kim, J. Wuenschell, S. P. Sharma, Ping Lu, P. Ohodnicki and P. W. Leu, *Nanotechnology*, 2018, **29**, 42LT01.

13 K. Nojiri, *Dry Etching Technology for Semiconductors*, Springer, 2012.

14 S. H. Kang, B. Pokroy, L. Mahadevan and J. Aizenberg, *ACS Nano*, 2010, **4**, 6323–6331.

15 R. H. Tredgold, *Order in Thin Organic Films*, Cambridge University Press, 1994.

16 S. A. Mahadik, M. S. Kavale, S. K. Mukherjee and A. V. Rao, *Applied Surface Science*, 2010, **257**, 333–339.

17 D. Nanda, P. Varshney, M. Satapathy, S. S. Mohapatra and A. Kumar, *Colloids and Surfaces A: Physicochemical and Engineering Aspects*, 2017, **529**, 231–238.

18 J. X. H. Wong and H.-Z. Yu, *J. Chem. Educ.*, 2013, **90**, 1203–1206.

19 A. D1003-13, *ASTM International*.

20 M.-H. Jung and H.-S. Choi, *Korean Journal of Chemical Engineering*, 2009, **26**, 1778–1784.

21 B. Bhushan, Y. C. Jung and K. Koch, *Langmuir*, 2009, **25**, 3240–3248.

22 J. Lomga, P. Varshney, D. Nanda, M. Satapathy, S. S. Mohapatra and A. Kumar, *Journal of Alloys and Compounds*, 2017, **702**, 161–170.

23 D. Ebert and B. Bhushan, *Langmuir*, 2012, **28**, 11391–11399.

24 M. Jurak and E. Chibowski, *Langmuir*, 2007, **23**, 10156–10163.

25 P. Mazumder, Y. Jiang, D. Baker, A. Carrilero, D. Tulli, D. Infante, A. T. Hunt and V. Pruneri, *Nano Letters*, 2014, **14**, 4677–4681.